TCAD Analysis of GaN HEMT Output Conductance Through Trap Rate Equation Green's Functions

TCAD Analysis of GaN HEMT Output Conductance Through Trap Rate Equation Green's Functions

Eva Catoggio
Dip. di Elettronica e Telecomunicazioni
Politecnico di Torino
Torino, Italy
eva.catoggio@polito.it

Simona Donati Guerrieri
Dip. di Elettronica e Telecomunicazioni
Politecnico di Torino
Torino, Italy
simona.donati@polito.it

Fabrizio Bonani
Dip. di Elettronica e Telecomunicazioni
Politecnico di Torino
Torino, Italy
fabrizio.bonani@polito.it

***Abstract*—An efficient, in-house developed, TCAD simulator is used to investigate the effects of buffer traps in 150 nm gate length GaN HEMTs. The developed TCAD allows to compute not only the sensitivity of DC and AC Y parameters towards variations of the trap physical parameters, but also the *local sensitivity*, showing the device areas where traps influence most the HEMT behavior. The technique is applied to analyze the dependency of the output impedance (Y_{DD}) of a Fe-doped HEMT versus the buffer trap energy and concentration. We demonstrate that the two trap parameters impact differently on the output resistance in terms of frequency dispersion and of absolute values. The local source is also different, showing that buffer trap energy variations are also important when traps are located below the saturated channel, while trap concentration perturbations are important only for traps located under the ohmic portion of the channel.**

***Index Terms*—GaN HEMTs, Nonlinear device models, TCAD simulations, Trap rate equations**

I. Introduction

The investigation of trap dynamics in GaN HEMT technology is necessary to mitigate their detrimental effects, that ultimately limit the microwave performances and the device reliability [1]. Signatures of traps are found in the HEMT dynamic behavior, e.g., in the gate and drain lag, i.e., the terminal current delay in response to voltage steps or pulses [2], [3], or in the peculiar low frequency dispersion of the device Y parameters [4]–[6]. While characterization results show that multiple traps are present in up-to-date GaN technologies, especially when buffer (Fe or C) doping is used, it is often cumbersome to identify the trap localization (buffer, surface, interface etc.) and their effect on the overall device electrical behavior. TCAD analysis represents a unique opportunity to link trap parameters and trap localization to the overall terminal characteristics, especially when trap density varies in the device volume.

In this scenario, it is extremely important to develop numerically efficient codes that can be used to simulate the device behavior, concurrently varying multiple trap parameters as well as position. An in-house software has been recently demonstrated allowing for 1) calculating the device solution varying the trap parameters starting from "nominal" trap values with negligible numerical overhead, and 2) extracting the *local sensitivity* for DC and AC parameters, i.e., identifying the regions of the device where the variations of trap parameters impact more the terminal characteristics. The method is described in detail in [7], where a preliminary demonstration has been given for the analysis of the GaN HEMT Y parameter dispersion as a function of the energy of GaN buffer traps. Here we extend the analysis to variations of the trap concentration and highlight that the variation of trap energy and concentration produces marked differences in terms of output impedance frequency dispersion and local variations.

This work has been supported by the Italian Ministero dell'Istruzione, dell'Università e della Ricerca (MIUR) under the PRIN 2017 Project "Empowering GaN-on-SiC and GaN-on-Si technologies for the next challenging millimeter-wave applications (GANAPP)".

II. Trap dynamic model implementation

In the in-house TCAD, a Trap Rate Equation (TRE) is added for each trap and coupled to the drift-diffusion (DD) transport model, forming the DD-TRE system as detailed in [7].

The DD-TRE model solution is implemented in the frequency domain by means of the harmonic balance (HB) approach [8], [9]. HB exploits a phasor-like formulation, having as unknowns the phasors of the physical internal variables, and it yields the terminal current phasors as a function of the external voltage generator phasors. For AC analysis and considering each device terminal (here denoted through terminal index r), the external generators correspond to the superposition of a DC component $V_0^{(r)}$, and of a small-amplitude tone at frequency ω with phasor $V_1^{(r)}$. Similarly, the terminal current is decomposed as the DC component $I_0^{(r)}$ and the AC phasor $I_1^{(r)}$, so that the (q,r) element of the device Y matrix can be expressed as

$$Y_{q,r} = \frac{I_1^{(q)}}{V_1^{(r)}} \tag{1}$$

Furthermore, the Y matrix element variation due to a perturbation of model parameters, e.g. trap concentration and/or energy, can be expressed as (Ω is the device volume)

$$\Delta Y_{q,r} = \frac{\Delta I_1^{(q)}}{V_1^{(r)}} = \sum_{\alpha} \int_{\Omega} K_{\alpha}^{(q,r)} \, \mathbf{dr} \tag{2}$$

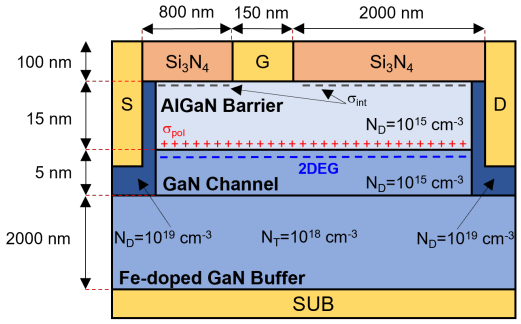

Fig. 1. Simulated HEMT structure.

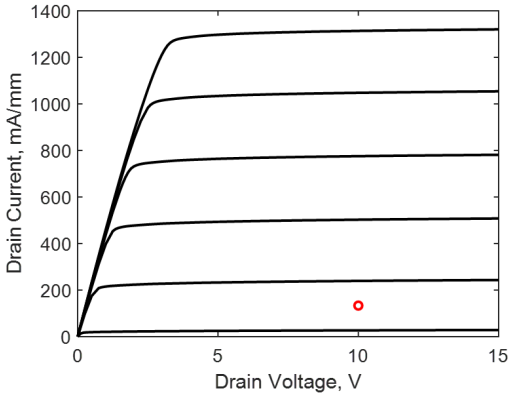

Fig. 2. Static characteristics varying the gate voltage from -2.5 V to 0 V with a step of 0.5 V. The red circle represents the quiescent bias point used for the AC analysis.

where $K_\alpha^{(q,r)}$ is the *distributed variation source* for equation α (Poisson, continuity or trap equation), which is in turn calculated following the Green's function approach [7].

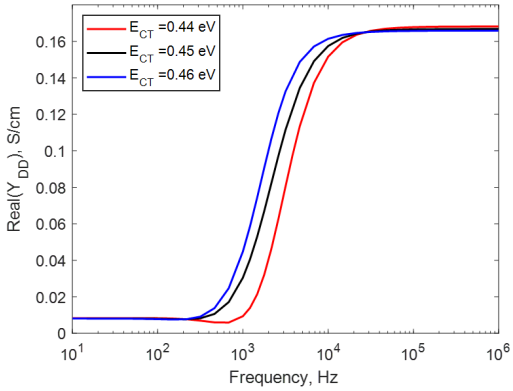

Fig. 3. Real part of Y_{DD} with varying trap energy levels [7]. $E_{CT} = 0.45$ eV is the nominal condition.

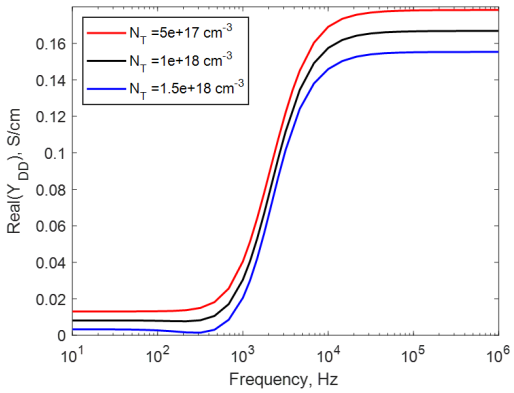

Fig. 4. Real part of Y_{DD} with varying trap concentration. $N_T = 10^{18}$ cm^{-3} is the nominal condition.

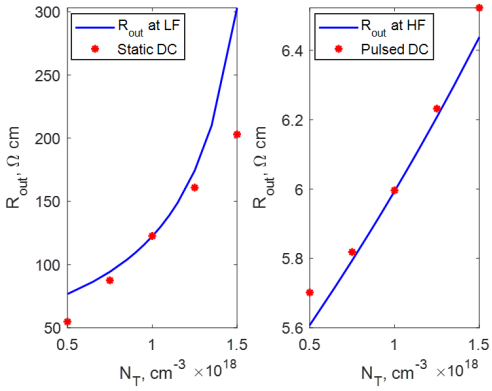

Fig. 5. Output resistance as a function of the trap concentration. Left: low frequency. Right: high frequency.

III. Device Structure

We simulate the 150 nm gate length HEMT shown in Fig. 1, made of an AlGaN barrier with 25% Al mole fraction, and of a GaN layer with a residual donor doping of 10^{15} cm^{-3}. The channel region, 5 nm thick, is placed above a 2 μm deep buffer characterized by Fe-induced deep acceptor-like traps with concentration $N_T = 10^{18}$ cm^{-3}, nominal energy $E_T = E_C - 0.45$ eV (E_C is the conduction band edge), and electron and hole capture cross-sections $\sigma_n = \sigma_p = 3 \times 10^{-16}$ cm^{-3}. Simulations include GaN spontaneous polarization and both the AlGaN spontaneous and piezoelectric polarization. The net polarization charge at the AlGaN/GaN interface is $\sigma_{\mathrm{pol}}/q = 1.34 \times 10^{13}$ cm^{-2} with 90% activation, while the polarization charge at the interface with contacts and passivation layers is exactly compensated. The in-house software implements the same polarization model as the Synopsys `Simplified strain model` [10]. Furthermore, a fixed negative charge $\sigma_{\mathrm{int}}/q = -2 \times 10^{12}$ cm^{-2} is added at the barrier/passivation interface, while surface interface traps are not included. See [7] for further details on the simulation settings.

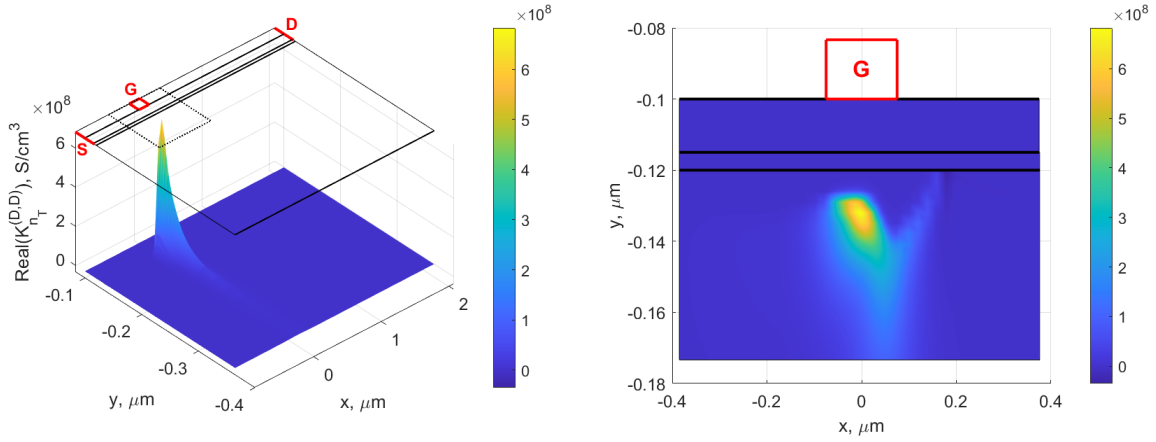

Fig. 6. Left: 3D plot of the real part of the distributed variation source $K_{n_T}^{(D,D)}$ due to E_{CT} variation [7]. Right: zoom of the dotted region under gate.

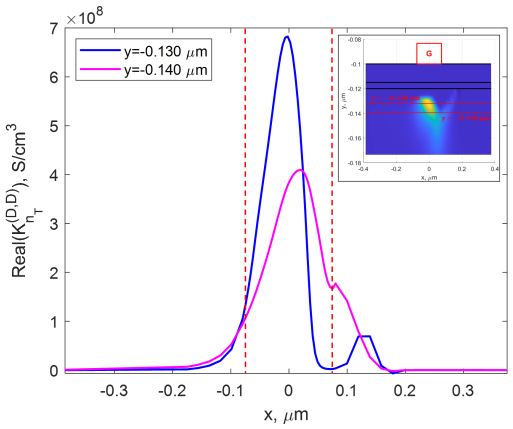

Fig. 7. Real part of $K_{n_T}^{(D,D)}$ due to E_{CT} variation along the x-axis extracted for $y = -0.130$ μm and $y = -0.140$ μm. The red dashed lines delimit the region under the gate.

IV. Results

First, the GaN HEMT structure is simulated in static conditions. Fig. 2 shows the DC output characteristics of the nominal device, characterized by a maximum saturation current of 1300 mA/mm. We investigate the effect of Fe trap dynamics on the HEMT output admittance Y_{DD}. The DC bias point, marked in Fig. 2 by the red circle, is set to $V_{\mathrm{DS}} = 10$ V and $V_{\mathrm{GS}} = -2.22$ V, corresponding to 10% of $I_{D\mathrm{ss}}$. Despite the lower drain voltage with respect to the one typically exploited for power applications (e.g., 28 V), this operating condition is similar to a class AB bias point and it allows for a direct comparison against experimental data [6]. Y_{DD} is extracted applying a 1 mV input tone at the drain contact whose frequency is swept from 1 Hz to 1 MHz. At each frequency, ΔY_{DD} is calculated according to (2) varying two trap parameters: $E_{CT} = E_C - E_T$ in the range $[0.44 - 0.46]$ eV and N_T in the interval $\pm 50\% N_T$. Fig. 3 and 4 show, as expected, the output admittance dispersion resulting from trap dynamics, with a significant increase at high frequencies, i.e., a reduced output resistance $R_{\mathrm{out}} = 1/\mathrm{Real}(Y_{\mathrm{DD}})$. Concerning parametric variations, $\mathrm{Real}(Y_{\mathrm{DD}})$ is almost insensitive to trap energy (Fig. 3) both at low (LF) and high frequency (HF), while the transition from LF to HF is shifted towards higher frequencies as E_T approaches E_C. The behavior is different varying the concentration N_T (Fig. 4): $\mathrm{Real}(Y_{\mathrm{DD}})$ is strongly affected at both low and high frequencies, increasing with decreasing trap concentration. To further demonstrate the model consistency, Fig. 5 (left) compares the output resistance extracted from the LF Y_{DD} with the one obtained from the slope of the static DC characteristics. Both models are found in agreement for all the considered N_T values. Similarly, Fig. 5 (right) reports the output resistance from the HF Y_{DD} value, demonstrating that it is consistent with the slope of the *pulsed* DC characteristic. Pulsed DC simulations are performed by the in-house solver freezing the trap concentration at the DC bias point (see [7] for details). For a more in-depth analysis of the output conductance behavior, we investigate the distributed variation $K_{\alpha}^{(D,D)}$ (see (2)) due to variations of the trap energy or concentration. The dominant contribution to ΔY_{DD} is found to be the distributed source of the trap rate equation $K_{n_T}^{(D,D)}$. The analysis is carried out at 2.15 kHz, where the variation vs. E_T is large. Fig. 6 shows the real part of $K_{n_T}^{(D,D)}$ due to a varied trap energy $E_T = E_C - 0.46$ eV (-10 meV from the nominal value). The distributed source is always positive and mainly extends from the source side to the mid-channel region under the gate contact. A milder impact is observed between gate and drain. Below the channel, located at $y = -0.115$ μm, traps are fully occupied down to $y = -0.125$ μm with negligible effect of energy variations. The distributed source is shifted instead more in depth into the buffer, up to 50 nm from the channel, presenting a sharp peak around $y = -0.130$ μm (see Fig. 6, right). Two cross-sections of $\mathrm{Real}(K_{n_T}^{(D,D)})$ at $y = -0.130, -0.140$ μm and reported in Fig. 7, show the distributed source along the x axis. Notice that it peaks under the gate from source to mid-channel, but it extends towards the drain below the saturated portion of the channel with

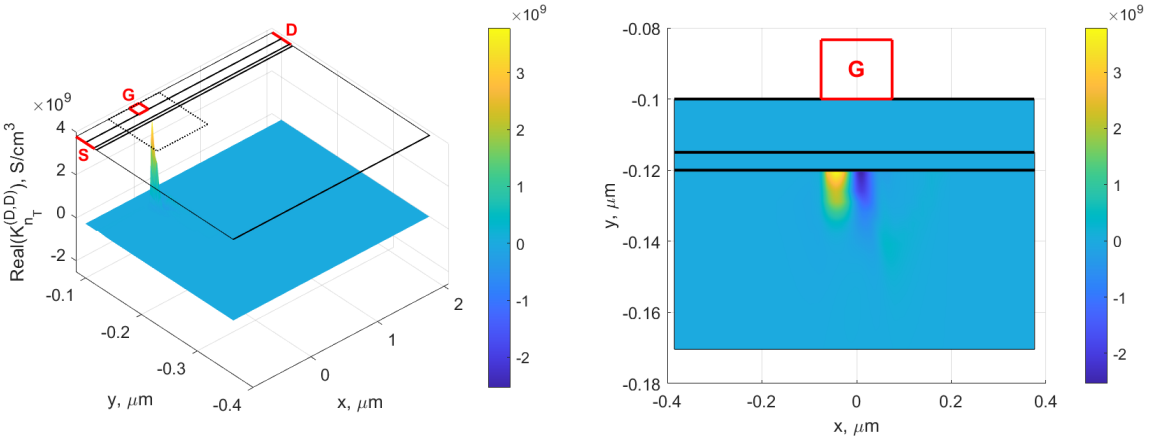

Fig. 8. Left: 3D plot of the real part of the distributed variation source $K_{n_T}^{(D,D)}$ due to N_T variation. Right: zoom of the dotted region under gate.

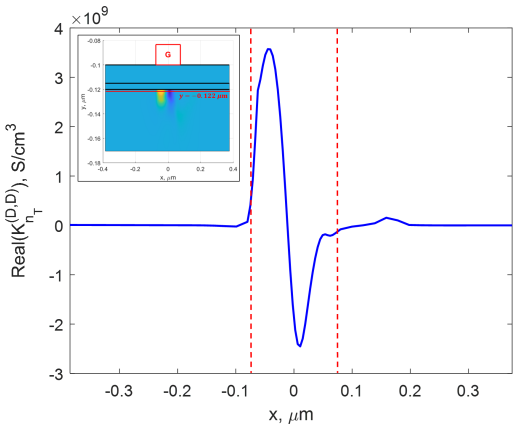

Fig. 9. Real part of $K_{n_T}^{(D,D)}$ due to N_T variation along the x-axis extracted for $y = -0.122$ μm. The red dashed lines delimit the region under the gate.

increasing depth. A more limited impact is observed in the area between the gate and drain contacts.

Fig. 8 shows marked differences in the case of trap concentration variations ($-50\%N_T$ from the nominal value). The distributed source is mainly localized at the top of the buffer region (see Fig. 8, right) since it is directly affected by N_T variations. Concerning variations in the x direction, a cross-section at $y = -0.122$ μm is reported in Fig. 9: differently fron energy variations, we notice a positive peak towards the source and a negative peak in the mid-channel region, while the area under the last portion of the channel and between gate and drain do not have any influence.

V. Conclusion

We exploited an in-house simulator, implementing the drift-diffusion model coupled to the trap rate equations, for the investigation of the AC output conductance towards the variation of trap physical parameters, i.e., trap energy and concentration. In particular, we demonstrated that the two trap parameters have a markedly different impact on the frequency dispersion behavior of the output impedance. The different trends can be traced back to the microscopic level, through the extraction of the local sensitivity, providing a further comprehension of the Y_{DD} behavior.

References

[1] G. Meneghesso, G. Verzellesi, F. Danesin, F. Rampazzo, F. Zanon, A. Tazzoli, M. Meneghini, E. Zanoni. "Reliability of GaN High-Electron-Mobility Transistors: State of the Art and Perspectives," *IEEE Trans. Device Mater. Reliab*, 8 (2), pp. 332–343, 2008, DOI: 10.1109/TDMR.2008.923743.

[2] N. Zagni, G. Verzellesi, A. Chini. "Temperature-Independent Current Dispersion in 0.15 μm AlGaN/GaN HEMTs for 5G Applications," *Micromachines*, 13 (12), p. 2244, 2022, DOI: 10.3390/mi13122244.

[3] A. M. Angelotti, G. P. Gibiino, A. Santarelli, C. Florian. "Experimental Characterization of Charge Trapping Dynamics in 100-nm AlN/GaN/AlGaN-on-Si HEMTs by Wideband Transient Measurements," *IEEE Transactions on Electron Devices*, 67 (8), pp. 3069-3074, 2020, DOI: 10.1109/TED.2020.3000983.

[4] P. Beleniotis, F. Schnieder,S. Chevtchenko, M. Rudolph. "Localization of Trapping Effects in GaN HEMTs with Pulsed S-parameters and Compact Models," in *2022 17th European Microwave Integrated Circuits Conference (EuMIC)*, DOI: 10.23919/EuMIC54520.2022.9923511.

[5] J. L. Gomes, L. C. Nunes, J. C. Pedro. "Transient Pulsed S-Parameters for Trapping Characterization," in *2020 International Workshop on Integrated Nonlinear Microwave and Millimetre-Wave Circuits (INMMiC)*, DOI: 10.1109/INMMiC46721.2020.9160297.

[6] P. V. Raja, N. K. Subramani, F. Gaillard, M. Bouslama, R. Sommet, J. C. Nallatamby. "Identification of Buffer and Surface Traps in Fe-Doped AlGaN/GaN HEMTs Using Y21 Frequency Dispersion Properties," *Electronics*, 10 (24), p. 3096, 2021, DOI: 10.3390/electronics10243096.

[7] E. Catoggio, S. Donati Guerrieri, F. Bonani. "TCAD Modeling of GaN HEMT Output Admittance Dispersion through Trap Rate Equation Green's Functions," *Electronics*, 12 (11), pp. 2457, 2023, DOI: 10.3390/electronics12112457.

[8] F. Bonani, S. Donati Guerrieri, G. Ghione, M. Pirola: "A TCAD approach to the physics-based modeling of frequency conversion and noise in semiconductor devices under large-signal forced operation," *IEEE Transactions on Electron Devices*, 48 (5), pp. 966-977, 2001, DOI: 10.1109/16.918245.

[9] F. Bertazzi, F. Bonani, S. Donati Guerrieri, G. Ghione. "Physics-based SS and SSLS variability assessment of microwave devices through efficient sensitivity analysis," in *2012 Workshop on Integrated Nonlinear Microwave and Millimetre-Wave Circuits (INMMIC)*, DOI: 10.1109/INMMIC.2012.6331920

[10] [Online]. Available: https://www.synopsys.com/silicon/tcad/device-simulation/sentaurus-device.html